Uniaxial and Biaxial Substrate Effects on Finline Characteristics

HUNG-YU YANG AND NICÓLAOS G. ALEXÓPOULOS, SENIOR MEMBER, IEEE

Abstract—**The effect of uniaxial and biaxial substrates on the frequency-dependent properties of a bilateral finline is investigated in this article. The finline characteristics are obtained by using the spectral-domain procedure in conjunction with the Galerkin method. Investigation of uniaxial substrates indicates that there is a particular optical axis direction for which the permittivity component in that direction dominates the finline behavior. In addition, a study has been carried out which determines the error which results when the material layer anisotropy is neglected.**

I. Introduction

THE FINLINE is a waveguiding structure which is increasingly used as a millimeter-wave component due to its various advantages such as reducing size, weight, and cost and in addition because it interfaces easily with other millimeter-wave circuits [1]. Uniform finline structures have been analyzed for isotropic substrates by many authors [2]–[6].

Anisotropy is present in a variety of practical substrates [7]. In addition, if it is neglected, the finline dispersion models developed with the aforementioned techniques will be in error, which will in general increase with increasing frequency for a given substrate thickness. The motivation of the present work is to develop a model which is highly accurate and which is capable of analyzing uniaxial or biaxial anisotropic substrate effects on the finline properties. In this article, the anisotropic substrates under consideration are characterized by a diagonalized tensor permittivity, i.e., they are either uniaxial or biaxial. In both cases, Maxwell's equations result in a pair of coupled wave equations which, when transformed into the Fourier domain, can be reduced to a fourth-order ordinary differential equation which is amenable to a straightforward solution. The spectral-domain approach is found here to yield an easy method to analyze anisotropic substrate effects because it deals with the Fourier coefficients of various field quantities separately rather than handling the total fields, as required when a solution is attempted in the space domain.

Numerical results are obtained by adopting the Galerkin method for the propagation constant of the dominant as well as higher order modes and for the finline characteristic impedance for both uniaxial and biaxial substrates. Of particular interest are the results obtained when the optical axis of a uniaxial substrate is oriented in different directions, since this highlights the importance of anisotropic effects on finline characteristics. In addition, the performed numerical analysis clarifies the error incurred if anisotropy is neglected.

Manuscript received April 14, 1986; revised August 21, 1986. This work was supported in part by the NSF under Grant ESC 82 15408 and Micro-TRW Research under Grant 85-129.

The authors are with the Electrical Engineering Department, University of California, Los Angeles, CA 90024.

IEEE Log Number 8611391.

II. Analytical Formulation

Although the methods adopted here can be applied to other structures, including unilateral finline, antipodal finline, or shielded microstripline and suspended substrate lines, here the problem is formulated for the bilateral finline only. The cross section of the structure under consideration is shown in Fig. 1(a). The substrate used is in general biaxial with a permittivity tensor assumed to be of the form

$$\hat{\epsilon} = \epsilon_0 \begin{bmatrix} \epsilon_{xx} & 0 & 0 \\ 0 & \epsilon_{yy} & 0 \\ 0 & 0 & \epsilon_{zz} \end{bmatrix}$$

where ϵ_0 is the free-space permittivity. The permeability of the substrate is assumed to be μ_0, which is the same as that in free space. The substrate is centered in the waveguide and the printed fin thickness is negligible.

With the permittivity in tensor form, the wave equations in the substrate can be derived from Maxwell's equations. In general, the wave equations are coupled partial differential equations given by

$$\frac{\epsilon_{yy}}{\epsilon_{xx}}\frac{\partial^2 E_y}{\partial y^2} + \frac{\partial^2 E_y}{\partial x^2} + \frac{\partial^2 E_y}{\partial z^2} - \left(1 - \frac{\epsilon_{zz}}{\epsilon_{xx}}\right)\frac{\partial^2 E_z}{\partial y\,\partial z} + k_0^2 \epsilon_{yy} E_y = 0 \tag{1a}$$

$$\frac{\epsilon_{zz}}{\epsilon_{xx}}\frac{\partial^2 E_z}{\partial z^2} + \frac{\partial^2 E_z}{\partial x^2} + \frac{\partial^2 E_z}{\partial y^2} - \left(1 - \frac{\epsilon_{yy}}{\epsilon_{xx}}\right)\frac{\partial^2 E_y}{\partial y\,\partial z} - k_0^2 \epsilon_{zz} E_z = 0 \tag{1b}$$

and

$$\epsilon_{xx}\frac{\partial E_x}{\partial x} - \epsilon_{yy}\frac{\partial E_y}{\partial y} + \epsilon_{zz}\frac{\partial E_z}{\partial z} = 0. \tag{1c}$$

The finline in the waveguide is excited by the dominant TE_{10} mode of the empty waveguide. Therefore, because of symmetry, a magnetic wall can be put at $x = -a_x$, and therefore only the half-structure shown in Fig. 1(b) need be considered. The field dependence $e^{j\omega t - j\beta z}$ is omitted

0018-9480/87/0100-0024$01.00 ©1987 IEEE

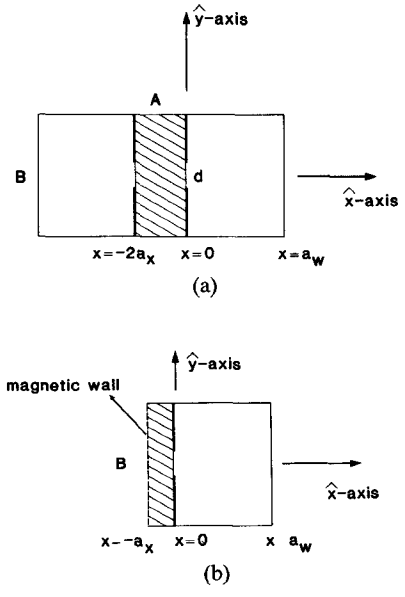

Fig. 1. (a) Cross section of the finline in waveguide. (b) Reduced geometry.

throughout this paper. The detailed procedure of the spectral-domain method has been reported previously [5], [6] and therefore only the important results are presented here. All the field quantities are Fourier transformed via

$$\begin{Bmatrix} \tilde{E}(n,x) \\ \tilde{H}(n,x) \end{Bmatrix} = \int_{-b/2}^{b/2} \begin{Bmatrix} E(x,y) \\ H(x,y) \end{Bmatrix} e^{jk_n y}\, dy \tag{2}$$

where

$$k_n = \begin{cases} 2n\pi/b, & n=0,1,2,\cdots \text{ for } E_z \text{ odd mode} \\ (2n-1)\pi/b, & n=1,2,3,\cdots \text{ for } E_z \text{ even mode.} \end{cases}$$

A. Region I — Anisotropic Region

If the Fourier transform defined in (2) is carried out for (1a), (1b), the following equations are obtained:

$$\frac{d^2\tilde{E}_y}{dx^2}(x,n) + g_1\tilde{E}_y(x,n) + g_2\tilde{E}_z(x,n) = 0$$
$$\frac{d^2\tilde{E}_z}{dx^2}(x,n) + e_1\tilde{E}_z(x,n) + e_2\tilde{E}_y(x,n) = 0 \tag{3}$$

where

$$e_1 = k_0^2\epsilon_{zz} - \beta^2\frac{\epsilon_{zz}}{\epsilon_{xx}} - k_n^2$$
$$e_2 = \left(1 - \frac{\epsilon_{yy}}{\epsilon_{zz}}\right)k_n\beta$$
$$g_1 = k_0^2\epsilon_{yy} - \frac{\epsilon_{yy}}{\epsilon_{xx}}k_n^2 - \beta^2$$
$$g_2 = \left(1 - \frac{\epsilon_{zz}}{\epsilon_{xx}}\right)k_n\beta. \tag{4}$$

As can be observed from (3), the field components are in general coupled together. But for $n=0$, $e_2 = g_2 = 0$, $E_x = E_z = 0$, and the electric-field components are decoupled. Subsequently, a solution is obtained in the form

$$\tilde{E}_{y1}(x, n=0) = A_0'\cos\beta_0(x+a_x)$$
$$\tilde{H}_{z1}(x, n=0) = \frac{\beta_0}{j\omega\mu_0}A_0'\sin\beta_0(x+a_x)$$
$$\tilde{H}_{x1}(x, n=0) = \frac{-\beta}{\omega\mu_0}A_0'\cos\beta_0(x+a_x) \tag{5}$$

where

$$\beta_0 = \sqrt{k_0^2\epsilon_{yy} - \beta^2}.$$

For $n \neq 0$, elimination of $\tilde{E}_y(x,n)$ in (3) yields

$$\frac{d^4}{dx^4}\tilde{E}_z(x,n) + (e_1+g_1)\frac{d^2}{dx^2}\tilde{E}_z(x,n) + (e_1g_1 - e_2g_2)\tilde{E}_z(x,n) = 0. \tag{6}$$

From (5) together with (3) and (1c) and the boundary conditions that $\tilde{H}_{y1}$, $\tilde{H}_{z1}$, $\tilde{E}_{x1}$ must be zero at $x = -a_x$, the total field expressions for region (I) are

$$\tilde{E}_{x1}(x,n) = s_7A_n'\sin\beta_{n1}(x+a_x) + s_8B_n'\sin\beta_{n2}(x+a_x)$$
$$\tilde{E}_{y1}(x,n) = s_1A_n'\cos\beta_{n1}(x+a_x) + s_2B_n'\cos\beta_{n2}(x+a_x)$$
$$\tilde{E}_{z1}(x,n) = A_n'\cos\beta_{n1}(x+a_x) + B_n'\cos\beta_{n2}(x+a_x)$$
$$\tilde{H}_{x1}(x,n) = \frac{-1}{j\omega\mu_0} \cdot [s_9A_n'\cos\beta_{n1}(x+a_x) + s_{10}B_n'\cos\beta_{n2}(x+a_x)]$$
$$\tilde{H}_{y1}(x,n) = \frac{-1}{j\omega\mu_0} \cdot [s_5A_n'\sin\beta_{n1}(x+a_x) + s_6B_n'\sin\beta_{n2}(x+a_x)]$$

and

$$\tilde{H}_{z1}(x,n) = \frac{-1}{j\omega\mu_0} \cdot [s_3A_n'\sin\beta_{n1}(x+a_x) + s_4B_n'\sin\beta_{n2}(x+a_x)] \tag{7}$$

where

$$\beta_{n1} = \sqrt{\frac{(e_1+g_1) + \sqrt{(e_1-g_1)^2 + 4e_2g_2}}{2}}$$
$$\beta_{n2} = \sqrt{\frac{(e_1+g_1) - \sqrt{(e_1-g_1)^2 + 4e_2g_2}}{2}}$$
$$s_1 = \frac{\beta_{n1}^2 - e_1}{e_2}, \qquad s_2 = \frac{\beta_{n2}^2 - e_1}{e_2}$$
$$s_3 = -s_1\beta_{n1} + \frac{jk_n}{\beta_{n1}}\left[\left(\frac{\epsilon_{yy}}{\epsilon_{xx}}\right)jk_ns_1 + \frac{\epsilon_{zz}}{\epsilon_{xx}}j\beta\right]$$
$$s_4 = -s_2\beta_{n2} + \frac{jk_n}{\beta_{n2}}\left[\left(\frac{\epsilon_{yy}}{\epsilon_{xx}}\right)jk_ns_2 + \frac{\epsilon_{zz}}{\epsilon_{xx}}j\beta\right]$$

and

$$s_5 = \frac{-j\beta}{\beta_{n1}}\left[\frac{\epsilon_{yy}}{\epsilon_{xx}}(jk_n)s_1 + \frac{\epsilon_{zz}}{\epsilon_{xx}}(j\beta)\right] + \beta_{n1}$$

$$s_6 = \frac{-j\beta}{\beta_{n2}}\left[\frac{\epsilon_{yy}}{\epsilon_{xx}}(jk_n)s_2 + \frac{\epsilon_{zz}}{\epsilon_{xx}}(j\beta)\right] + \beta_{n2}$$

$$s_7 = \frac{1}{\beta_{n1}}\left[\frac{\epsilon_{yy}}{\epsilon_{xx}}(jk_n)s_1 + \frac{\epsilon_{zz}}{\epsilon_{xx}}j\beta\right]$$

$$s_8 = \frac{1}{\beta_{n2}}\left[\frac{\epsilon_{yy}}{\epsilon_{xx}}(jk_n)s_2 + \frac{\epsilon_{zz}}{\epsilon_{xx}}j\beta\right]$$

$$s_9 = -\frac{jk_n s_5 + j\beta s_3}{\beta_{n1}}$$

$$s_{10} = -\frac{jk_n s_6 + j\beta s_4}{\beta_{n1}}. \tag{8}$$

B. Region II — Air Region

In this region, the fields are composed of both TE and TM modes which have been reported by [5] and [6]; only the results are given here

$$\tilde{E}_{x2}(x,n) = \left[\frac{\omega\mu_0}{\beta}(-jk_n)A_n + k_x B_n\right]\cos k_x(x-a_w)$$

$$\tilde{E}_{y2}(x,n) = \left[\frac{\omega\mu_0}{\beta}k_x A_n - jk_n B_n\right]\sin k_x(x-a_w)$$

$$\tilde{E}_{z2}(x,n) = \frac{j(k_0^2-\beta^2)}{\beta}B_n \sin k_x(x-a_w)$$

$$\tilde{H}_{x2}(x,n) = \left[-k_x A_n + \frac{\omega\epsilon_0}{\beta}(jk_n)B_n\right]\sin k_x(x-a_w)$$

$$\tilde{H}_{y2}(x,n) = \left[-jk_n A_n + \frac{\omega\epsilon_0}{\beta}k_x B_n\right]\cos k_x(x-a_w)$$

and

$$\tilde{H}_{z2}(x,n) = \frac{j(k_0^2-\beta^2)}{\beta}A_n \cos k_x(x-a_w) \tag{9}$$

where

$$k_x = \sqrt{k_0^2-\beta^2-k_n^2}.$$

It is assumed that the Fourier transform of tangential $\bar{E}$-fields $E_{y0}(y)$, $E_{z0}(y)$ and currents $J_{y0}(y)$, $J_{z0}(y)$ on the air–dielectric interface region are denoted by $\tilde{E}_{y0}(n)$, $\tilde{E}_{z0}(n)$ and $\tilde{J}_{y0}(n)$, $\tilde{J}_{z0}(n)$, respectively, where E_{y0}, E_{z0} are zero in $|y| \geq w/2$ and J_{y0}, J_{z0} are zero in $|y| \leq w/2$. Applying the boundary conditions, the unknowns A_n', B_n', A_n, B_n are eliminated and the following two coupled algebraic equations are obtained:

$$Y_{11}(n,\beta)\tilde{E}_{y0}(n) + Y_{12}(n,\beta)\tilde{E}_{z0}(n) = -j\omega\mu_0\tilde{J}_{y0}(n) \tag{10a}$$

$$Y_{21}(n,\beta)\tilde{E}_{y0}(n) + Y_{22}(n,\beta)\tilde{E}_{z0}(n) = -j\omega\mu_0\tilde{J}_{z0}(n) \tag{10b}$$

where

$$Y_{11}(n=0) = -\left(\epsilon_{yy}k_0^2-\beta^2\right)\frac{\tan(\beta_0 a_x)}{\beta_0} + \left(k_0^2-\beta^2\right)\frac{\cot(k_x a_w)}{k_x}$$

$$Y_{12}(n=0) = Y_{21}(n=0) = Y_{22}(n=0) = 0$$

$$Y_{11}(n\neq 0) = \frac{s_3\tan(\beta_{n1}a_x) - s_4\tan(\beta_{n2}a_x)}{(s_1-s_2)} + \frac{k_0^2-\beta^2}{k_x}\cot(k_x a_w)$$

$$Y_{12}(n\neq 0) = \frac{s_1 s_4\tan(\beta_{n1}a_x) - s_2 s_3\tan(\beta_{n2}a_x)}{s_1-s_2} + \frac{\cot(k_x a_w)}{k_x}\beta k_n$$

$$Y_{21}(n\neq 0) = \frac{s_6\tan(\beta_{n2}a_x) - s_5\tan(\beta_{n1}a_x)}{s_1-s_2} + \frac{\cot(k_x a_w)}{k_x}\beta k_n$$

and

$$Y_{22}(n\neq 0) = \frac{s_2 s_5\tan(\beta_{n1}a_x) - s_1 s_6\tan(\beta_{n2}a_x)}{s_1-s_2} + \frac{k_0^2-k_n^2}{k_x}\cot(k_x a_w). \tag{11}$$

Subsequently, the Galerkin method is applied by first expanding $E_{y0}(y)$, $E_{z0}(y)$ in terms of a set of known functions $\xi_r(y)$, $\eta_s(y)$, i.e.,

$$\tilde{E}_{y0}(n) = \sum_{r=1}^{M} c_r\tilde{\xi}_r(n)$$

$$\tilde{E}_{z0}(n) = \sum_{s=1}^{N} d_s\tilde{\eta}_s(n) \tag{12}$$

where $\tilde{\xi}_r(n)$, $\tilde{\eta}_s(n)$ are the Fourier transforms of $\xi_r(y)$, $\eta_s(y)$. Substituting (12) into (10a) and (10b) and applying the inner product to the resulting equation with $\tilde{\xi}_p(n)$ and $\tilde{\eta}_q(n)$, respectively, the following equations are obtained:

$$\sum_{r=1}^{M} w_{pr}^{11}c_r + \sum_{s=1}^{N} w_{ps}^{12}d_s = 0, \qquad p = 1,2,3,\cdots$$

and

$$\sum_{r=1}^{M} w_{qr}^{21}c_r + \sum_{s=1}^{N} w_{qs}^{22}d_s = 0, \qquad q = 1,2,3,\cdots \tag{13}$$

where

$$w_{pr}^{11} = \tfrac{1}{2}\sum_{n=0}^{\infty}\delta_n\tilde{\xi}_p(n)Y_{11}(\beta,n)\tilde{\xi}_r(n)$$

and

$$w_{ps}^{12} = \sum_{n=0}^{\infty} \tilde{\xi}_p(n) Y_{12}(\beta, n) \tilde{\eta}_s(n)$$

$$w_{qr}^{21} = \sum_{n=0}^{\infty} \tilde{\eta}_q(n) Y_{21}(\beta, n) \tilde{\xi}_r(n)$$

$$w_{qs}^{22} = \sum_{n=0}^{\infty} \tilde{\eta}_q(n) Y_{22}(\beta, n) \tilde{\eta}_s(n) \tag{14}$$

where

$$\delta_n = \begin{cases} 1, & n = 0 \\ 2, & n \neq 0. \end{cases}$$

Equation (13) represents a homogeneous $(M+N)\times(M+N)$ matrix for the unknown coefficients c_r and d_s. For nontrivial solutions, the determinant of the matrix is equated to zero, which yields solutions for the propagation constants for the dominant as well as higher order modes. The characteristic impedance of the dominant mode is an important quantity in the design of microwave and millimeter-wave circuits. Since the field is not a TEM mode, the definition of characteristic impedance is not unique. Due to the reasons pointed out in [8], the power–voltage definition is most suitable for the finline structure, i.e.,

$$Z_c = \frac{V_{y0}^2}{2P} \tag{15}$$

where V_{y0} is the voltage between the fins and P is the average total power flow. These quantities are given by

$$V_{y_0} = \int_{-w/2}^{w/2} \sum_{r=1}^{M} c_r \xi_r(y)\, dy \tag{16}$$

and

$$P = 2\,\mathrm{Re} \int_{-a_x}^{a_w} \int_{-b/2}^{b/2} \left(E_x H_y^* - E_y H_x^*\right) dy\, dx.$$

The expansion coefficient c_r, d_s can be computed once the propagation constant of the dominant mode is obtained. Then the power flow can be calculated by applying Parseval's theorem to yield

$$P = \frac{1}{b}\tilde{P}(n=0) + \frac{2}{b}\sum_{n=1}^{\infty} \tilde{P}(n) \tag{17}$$

where

$$\tilde{P}(n) = \mathrm{Re} \int_{-a_x}^{a_w} \left(\tilde{E}_x \tilde{H}_y^* - \tilde{E}_y \tilde{H}_x^*\right) dx.$$

In order to obtain more accurate results using fewer terms, the basis functions are suitably chosen such that the edge condition can be incorporated, as suggested in [6].

As an example, the following expansions are chosen for the dominant mode:

$$\xi_r(y) = \frac{\cos\left[(r-1)\pi\left(\dfrac{y}{w/2}\right)\right]}{\sqrt{1-\left(\dfrac{y}{w/2}\right)^2}} \tag{18}$$

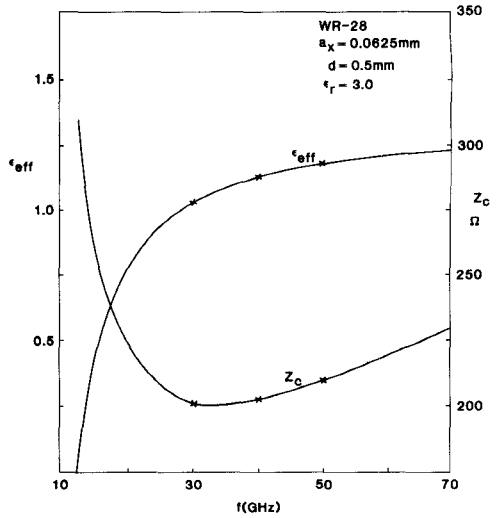

Fig. 2. Dispersion characteristics of the finline mode, x the results in [6].

and

$$\eta_s(y) = \frac{\sin\left[s\pi\left(\dfrac{y}{w/2}\right)\right]}{\sqrt{1-\left(\dfrac{y}{w/2}\right)^2}}. \tag{19}$$

III. Numerical Analysis

The numerical values of the effective dielectric constant, i.e., $\epsilon_{\mathrm{eff}} = (\beta/k_0)^2$, and characteristic impedance were first obtained for an isotropic material so as to compare these results with data available in the literature [6]. Excellent agreement has been obtained, as shown in Fig. 2. In general, three basis functions and 200 Fourier terms have provided excellent convergence and are in agreement with the discussions and conclusions in [6]. The anisotropic effects on the finline characteristics are theoretically investigated for $\epsilon_r = 3.0$ by changing dielectric constants in the x, y, and z directions to 3.5, respectively. The ϵ_{eff} computations show that the difference for $\epsilon_{xx} = 3.5$ is about 0.35 percent, for $\epsilon_{yy} = 3.5$ about 5 percent, and for $\epsilon_{zz} = 3.5$ less than 0.01 percent in WR-28 waveguide, over the frequency range of only the dominant-mode propagation.

The comparison is illustrated in Table I. It is interesting to observe that due to TE_{10} mode fed to the finline, in the propagation direction, the strength of E_z is much smaller than that of E_y and E_x. As a result, the anisotropic effect in the z-direction is almost negligible. Also, the substrate width is very small compared with the length of the waveguide broad wall (about 1.75 percent in our case); therefore, the anisotropic effect in the x-direction is much smaller than that in the y-direction. The propagation constant of the first higher order mode, which is important in the design of single-mode propagation, is also investigated. The comparison is illustrated in Table I.

Due to the fact that the substrate is very thin, most of

TABLE I
COMPARISON OF FINLINE CHARACTERISTICS OF KAPTON VERSUS ANISOTROPIC KAPTON

f(GHz)	ϵ_{eff}^{a}	ϵ_{eff}^{b}	Error	ϵ_{eff}^{c}	Error	Z_c^a	Z_c^b	Error	Z_c^c	Error
13	0 0977	0.1508	35.6%	0.1011	3.38%	618.6	497.8	24.3%	608.3	1.69%
30	1.0266	1.0843	5.32%	1.0302	0.35%	201.9	199.4	1.25%	201.8	0.%
40	1 1263	1.1872	5.13%	1.1300	0.33%	202.2	201.5	0.35%	202.2	0.%
50	1.1774	1.2420	5.20%	1.1814	0.34%	208.7	209.5	0.38%	208.7	0.%
	#0.1153	0.1238	6.80%	0.1158	0.43%					
60	1.2099	1.2797	5.38%	1.2141	0.35%	217.7	219.8	0.96%	217.9	0.%
	#0.3964	0.4034	1.73%	0.3969	0 13%					

WR-28, d=0.5mm, a_x=0.0625mm, # the first higher mode (a) $\epsilon_r = 3.0$,
(b) $\epsilon_{xx} = \epsilon_{zz} = 3.0$, $\epsilon_{yy} = 3.5$, (c) $\epsilon_{xx} = 3.5$, $\epsilon_{yy} = \epsilon_{zz} = 3.0$

TABLE II
COMPARISON OF FINLINE CHARACTERISTICS OF KAPTON VERSUS ANISOTROPIC KAPTON

W/A	ϵ_{eff}^{a}	ϵ_{eff}^{b}	Error	ϵ_{eff}^{c}	Error	Z_c^a	Z_c^b	Error	Z_c^c	Error
0 02	1.055	1 119	5.72%	1.059	0.4%	197.9	195 2	1.38%	197 8	0 %
0.04	1.246	1.351	7.71%	1.258	0 88%	172.0	168 3	2.20%	171 6	0.23%
0.08	1.486	1 632	8.95%	1.513	1 78%	141.5	137 1	3 1%	140 6	0 64%
0.16	1.724	1.905	9.50%	1 777	2.97	112.4	107.8	4.27%	111.1	1.17%
0.32	1.952	2.189	10.8%	2.023	3.54%	83.2	76 3	9.03%	82.3	1 09%

WR-28, d=0.5mm, W: the substrate thickness (a) ϵ_r 3.0,
(b) $\epsilon_{xx} = \epsilon_{zz} = 3.0$, $\epsilon_{yy} = 3.5$, (c) $\epsilon_{xx} = 3.5$, $\epsilon_{yy} = \epsilon_{zz} = 3.0$

the power is propagating in the air region, and this makes the characteristic impedance insensitive to the anisotropic effect. For single-mode frequency range, the finline has very much the same characteristics as the ridged waveguide. The characteristic impedance is sensitive to the change of propagation constant near the cutoff frequency, as pointed out by [8], and it is given by

$$Z_{oc} \sim \frac{Z_\infty}{\sqrt{1-(\lambda/\lambda_c)^2}}.$$

This explains why at lower frequencies the anisotropy has stronger effects on the characteristic impedance. This effect also is shown in Table I.

The effects of substrate anisotropy on the finline characteristics are also investigated with varying substrate thickness. The results are shown in Table II. It is observed that as substrate thickness increases, the error with neglecting substrate anisotropy becomes more severe. The comparison of sapphire as a substrate with the optical axis oriented in different directions is presented in Fig. 3. Due to the strong anisotropy, discrepancies of almost 21 percent for ϵ_{eff} and 9 percent for the characteristic impedance are observed at 15 GHz. The characteristics of finline for anisotropic PTFE [9] with $\epsilon_{xx} = 2.45$, $\epsilon_{yy} = 2.89$, $\epsilon_{zz} = 2.95$, and isotropic PTFE with $\epsilon_r = 2.45$ are shown in Fig. 4. It is of interest to see that the characteristic impedance curves

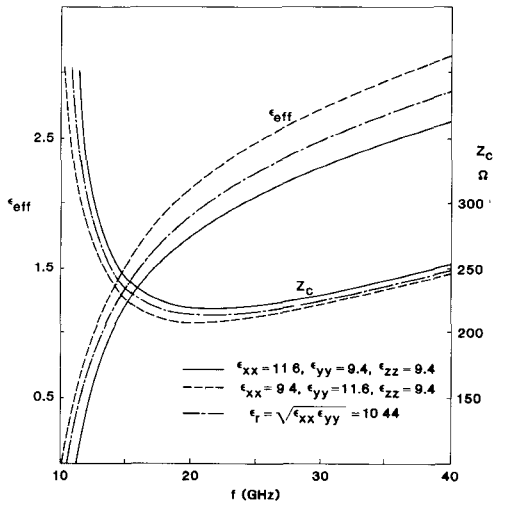

Fig. 3. Finline characteristics. WR-28, $a_x = 0.127$ mm, $d = 1$ mm.

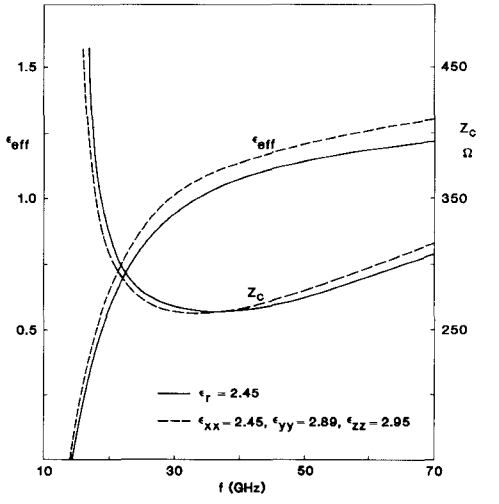

Fig. 4. Finline characteristics. WR-28, $a_x = 0.127$ mm, $d = 1$ mm.

for the above two substrates intersect at about 40 GHz. Above this frequency, the impedance for the case of the anisotropic substrate has larger values, while below this frequency, it has the lower value. This phenomenon depends on waveguide dimensions and substrate parameters.

IV. CONCLUSIONS

A theoretical and numerical analysis of the bilateral finline with an anisotropic substrate was presented. The propagation constant as well as characteristic impedance of the dominant mode was obtained by the spectral-domain approach and subsequent use of the Galerkin numerical procedure. The approach proved to yield excellent accuracy, and substrate materials such as sapphire and anisotropic PTFE were used to highlight the effect of anisotropy on ϵ_{eff} and Z_0. It was found that a significant error in computing ϵ_{eff} and Z_0 is incurred if anisotropy is neglected.

ACKNOWLEDGMENT

The authors wish to thank M. Schoneberg for typing the manuscript.

REFERENCES

[1] P. J. Meier "Integrated fin-line millimeter components," *IEEE Trans. Microwave Theory Tech.*, vol. MTT-22, pp. 1209–1216, Dec. 1974.

[2] H. Hofmann "Dispersion of planar waveguide for millimeter wave application," *Arch. Elek. Übertragung*, vol. 31, no. 1, pp. 40–44, Jan. 1977.

[3] A. M. A. El-Sherbiny, "Exact analysis of shielded microstrip lines and bilateral finline," *IEEE Trans. Microwave Theory Tech.*, vol. MTT-29, pp. 669–675, July 1981.

[4] D. Mirshekar-Syahkal and J. Brian Davies, "An accurate unified solution to various finline structures of phase constant, characteristic impedance, and attenuation," *IEEE Trans. Microwave Theory Tech.*, vol. 30, Nov. 1982.

[5] J. B. Knorr and P. M. Shagela, "Millimeter-wave finline characteristics," *IEEE Trans. Microwave Theory Tech.*, vol. MTT−28, pp. 737–743, July 1980.

[6] L.-P. Schmidt and T. Itoh, "Spectral domain analysis of dominant and higher order modes in finline," *IEEE Trans. Microwave Theory Tech.*, vol. MTT-28, pp. 981–985, Sept. 1980.

[7] N. G. Alexópoulos, "Integrated circuit structures on anisotropic substrates," *IEEE Trans. Microwave Theory Tech.*, vol. MTT-11, pp. 847–882, Oct. 1985.

[8] R. Jansen "Unified user-oriented computation of shielded covered and open planar microwave and millimeter wave transmission line characteristics," *Microwave Opt. Acoust.*, vol. 3, no. 1, pp. 40–42, Jan. 1979.

[9] M. Olyphant, Jr., "Measuring anisotropy in microwave substrate," in *IEEE MTT-S 1979 Int. Microwave Symp. Dig.*, Apr. 30–May 2, 1979, pp. 91–94.

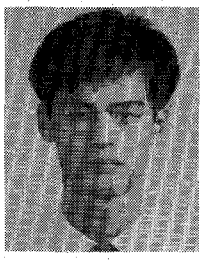

Hung-Yu Yang was born in Taipei, Taiwan, on October 25, 1960. He received the B.S. degree in electrical engineering from National Taiwan University in 1982 and the M.S. degree in electrical engineering from University of California at Los Angeles in 1985.

During 1982–1984, he served in R.O.C. Navy as an electronics officer. He is currently working towards the Ph.D. degree at the University of California at Los Angeles. His research interests are in printed-circuit antennas and the modeling of microwave and millimeter wave devices.

✠

Nicólaos G. Alexópoulos (S'68–M'69–SM'82) was born in Athens, Greece, in 1942. He graduated from the 8th Gymnasium of Athens, Greece, and subsequently obtained the B.S.E.E., M.S.E.E., and Ph.D. degrees from the University of Michigan, Ann Arbor, MI, in 1964, 1967, and 1968, respectively.

He is currently a Professor in the Department of Electrical Engineering, University of California, Los Angeles, and a Consultant with Northrop Corporation's Advanced Systems Division. His current research interests are in electromagnetic theory as it applies in the modeling of integrated-circuit components and printed circuit antennas for microwave and millimeter-wave applications, substrate materials and their effect on integrated-circuit structures and printed antennas, integrated-circuit antenna arrays, and antenna concealment studies. He is the Associate Editor of the IEEE TRANSACTIONS ON ANTENNAS AND PROPAGATION, *Electromagnetics Journal*, and *Alta Frequenza*.